ACS OMEGA

Article

Cite This: ACS Omega XXXX, XXX, XXX−XXX

http://pubs.acs.org/journal/acsodf

CO_2 Adsorption and Activation on the (110) Chalcopyrite Surfaces: A Dispersion-Corrected DFT + *U* Study

Rasoul Khaledialidusti,*[,†] Abhishek Kumar Mishra,*[,‡] and Afrooz Barnoush*[,†,§]

[†]Department of Mechanical and Industrial Engineering, NTNU, Trondheim 7491, Norway

[‡]Department of Physics, School of Engineering, University of Petroleum and Energy Studies, Bidholi via Premnagar, Dehradun 248007, UK, India

[§]Curtin Corrosion Centre WASM-MECE, Curtin University, Bentley, Australia

Supporting Information

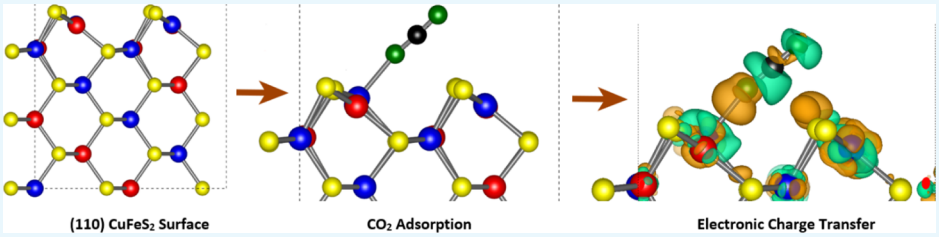

ABSTRACT: We have used the density functional theory within the plane-wave framework to understand the reconstruction of most stable (110) chalcopyrite surfaces. Reconstructions of the polar surfaces are proposed, and three different possible nonpolar terminations for the (110) surface, namely, I, II, and III, are investigated. A detailed discussion on stabilities of all three surface terminations is carried out. It is generally observed that the (110) chalcopyrite surfaces encounter significant reconstruction in which the metal Fe and Cu cations in the first atomic layer considerably move downward to the surface, while the surface S anions migrate slightly outward toward the surface. We also investigated the adsorption of the CO_2 molecule on the three terminations for the (110) surface by exploring various adsorption sites and configurations using density functional theory calculations, in which long-range dispersion interactions are taken into consideration. We show that the CO_2 molecule is adsorbed and activated, while spontaneous dissociation of the CO_2 molecule is also observed on the (110) surfaces. Structural change from a neutral linear molecule to a negatively charged ($CO_2^{-\delta}$) slightly or considerably bent species with stretched C−O bond distances are highlighted for description of the activation of the CO_2 molecule. The results address the potential catalytic activity of the (110) chalcopyrite toward the reduction and conversion of CO_2 to the organic molecule, which is appropriate to the production of liquid fuels.

1. INTRODUCTION

Transition-metal sulfides are the main class of Earth materials with an interesting variety of structure types[1] that have been technologically familiarized for different advanced functional material applications. Chalcopyrite ($CuFeS_2$) as one of these structure types reveals a host of industrially applicable electronic, magnetic, and catalytic properties. Chalcopyrite is known as a common mineral of noticeable economic applicability that is commercially the main source of copper, accounting for the majority of copper reserves in the world.[2]

Structurally, in chalcopyrite, each anion (sulfur atom) is bonded to four cations (two copper atoms and iron atoms), forming a tetrahedra.[3] Chalcopyrite is known as an antiferromagnetic (AFM) semiconductor material with spins on any two iron atoms bonded to a common sulfur atom are opposed and directed along the *c* axis[3] (Figure 1). The magnetic and electrical properties of chalcopyrite are still not completely known today. The electrical, structural, and in particular the band gap properties of chalcopyrite have made it as an interesting compound in a range of semiconductor applications such as optical devices,[4] photodiodes,[5] spintronic devices,[6] and thin-film intermediate-band solar cells.[7]

Because the properties of nanostructures deviate considerably from their bulk complement, a comprehensive understanding at the molecular level is required to design functional devices. Significant efforts have been performed toward understanding the chemistry and physics of chalcopyrite, and as a result of these studies, a variety of interesting properties have been discovered.[8−16] It is well understood that the catalytic properties are intensely affected by the surface structures. The connection between atomic-scale properties and the macroscopic functionality is an effective factor to modify catalytic surfaces,[17] and the first step is the adsorption of molecules on a catalyst surface through their activation and conversion.

Received: July 1, 2019
Accepted: September 9, 2019

DOI: 10.1021/acsomega.9b01988
ACS Omega XXXX, XXX, XXX−XXX

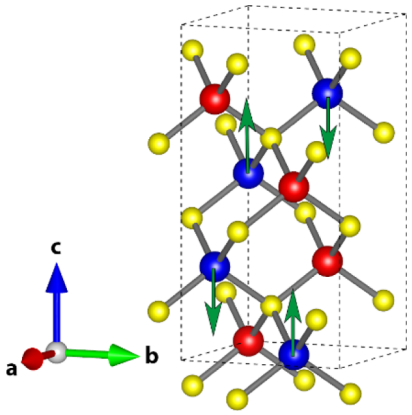

Figure 1. Schematic of the $CuFeS_2$ bulk structure. Red, blue, and yellow spheres represent the Cu, Fe, and S atoms, respectively. The S atoms are repeated in the edges because of the periodic boundary conditions.

A significant number of theoretical investigations were performed for exploring the capability of different $CuFeS_2$ surfaces on the adsorption of molecules.[8−14] Stirling et al.,[14] for example, analyzed the adsorption of H_2O on the (100) surface using the density functional theory (DFT) and plane wave basis set, and the strongest chemisorption energy obtained was almost −54 kJ/mol. In a similar study,[13] they studied the molecular adsorption of H_2S on the (100) surface, and it was presented that the adsorption is favorable with an adsorption energy of almost −46 kJ/mol. In addition, the H_2O adsorption on the (001) surface was studied by de Lima et al.[15] and they stated that the water adsorption on the iron atom is the preferred mechanism with an adsorption energy of almost −95 kJ/mol. They also studied the adsorption of sulphuric acid and hydrochloric acid on the relaxed $CuFeS_2$ (001) surface.[16] Other surfaces such as (111), (101), (110), and (112) were introduced as relevant surfaces for chalcopyrite and similar structures;[3,18−20] however, the (110) surface was found to be the most stable nonpolar surface.[21−23] Natarajan et al. studied the chemical and flotation behavior of chalcopyrite in the presence of *Acidithiobacillus thiooxidans* for the selective removal of pyrite from chalcopyrite for the economic extraction of valuable copper. Recently, Mikhlin et al.[24] have studied possible configurations arising at $CuFeS_2$(110) and (012) surfaces because of the removal of adjacent Fe atoms in the top layers by applying DFT calculations and also performed X-ray photoelectron spectroscopy studies of the chalcopyrite samples slightly oxidized in water.[25]

Carbon dioxide is known as the main source of the current climate changes.[26] The adverse influence of greenhouse gas emissions could be alleviated by CO_2 utilization. The synthesis product chemicals from CO_2 are not only a promising substitute to conventional fossil fuels but also it could improve the current technologies of carbon capture, sequestration, and storage.[27] A considerable number of efforts have been performed so far to realize the efficient ways of reducing CO_2 and converting it into organic molecules, which are the origins of fuel and chemical feedstocks.[27,28] The adsorption, activation, and conversion of CO_2 have been widely studied on metal−organic frameworks,[29−32] transition-metal complexes,[33,34] and metal-oxide surfaces.[35−40] For example, based on the previously performed theoretical studies, CO_2 adsorbs on FeS(001), FeS(011), and FeS(111) surfaces with an energy of −19.3, −0.73, and −83.9 (kJ/mol), respectively. CO_2 adsorbs exothermally with a binding energy of −71.4, −76, and −93.2 (kJ/mol) on CuO(111), CuO($\bar{1}$11), and CuO(011) surfaces, respectively. The adsorption energy of CO_2 on graphene is calculated in a range of 25−30 (kJ/mol) in the physisorption regime. In addition, CO adsorption and oxidation on Fe_3O_4 and Fe_4C surfaces are studied, and the results show that the adsorbed CO is partially negatively charged, indicating the improved electron transfer from the surfaces to CO, and the more the electron transfer, the stronger the CO activation.[41−43] Besides, the studies accomplished so far, to the best of our knowledge, there are no published studies of the adsorption, activation, and conversion of CO_2 on the chalcopyrite surfaces.

In the present study, the reactivity of the (110) chalcopyrite surface as the most stable surface appearing in the $CuFeS_2$ has been investigated extensively toward the adsorption and activation of CO_2 using DFT to realize the factors that have a great influence on the catalytic activity. To do this, first, a detailed first-principles-based study of different terminations of $CuFeS_2$(110) surfaces has been provided. The reconstruction and stability of the surfaces has been discussed by analyzing their structure properties and surface energies. Second, we have studied the CO_2 adsorption and activation on the terminated $CuFeS_2$(110) surfaces by interpreting the structural of different cases of adsorption. Different adsorption sites on the surfaces have been explored, aiming to contribute to understand the role of chalcopyrite for CO_2 adsorption and activation at a molecular level. Our results show that different terminated (110) surfaces can activate the CO_2 molecule. In addition, the results show the subsequent dissociation of the molecule to form CO and O species, which provide useful information in the expansion of more well-organized $CuFeS_2$ catalysts with reactive surfaces.

2. COMPUTATIONAL METHODOLOGY

Spin-polarized periodic DFT calculations have been carried out using the Vienna Ab initio Simulation Package (VASP) with a plane-wave basis set.[44−47] The DFT + U[48] methodology with the generalized gradient approximation using the exchange−correlation functional of Perdew, Burke, and Ernzerhof[49,50] and the formalism of Dudarev et al.[48] has been employed to capture the strong correlation effect of 3d electrons that are required for a more accurate description of the transition metals of Cu and Fe in chalcopyrite.[51,52]

Chalcopyrite crystalizes in the tetragonal group with the space group $I\bar{4}2d$ (D_{2d}^{12}).[51−53] The lattice constants determined by the X-ray diffraction experiment was found to be $a = b =$ 5.289[54] (5.286[55]) Å and c = 10.423[54] (10.410[55]) Å. In our previous study,[52] temperature-dependent properties (structure, mechanics, and thermodynamics) of magnetic $CuFeS_2$ were evaluated from first-principles calculations. The Hubbard correction term (i.e., the U_{eff} value)[48] was carefully chosen for the localized 3d electrons of Cu and Fe, where U_{eff} is the difference between the Coulomb U and exchange J parameters. Calculations including a Hubbard term for Fe atoms were executed with U_{eff} in intervals of 1 eV up to 9 eV with a constant Hubbard term for Cu atoms. Calculations with a different Hubbard term for Cu atoms did not have any significant effect on the relative energies of the considered states and the atomic populations. Different magnetic states of the AFM and FM phases for the supercells were analyzed, and the spin configurations corresponding to the AFM phases were

DOI: 10.1021/acsomega.9b01988
ACS Omega XXXX, XXX, XXX−XXX

initially assigned to the Fe atoms, as the most stable spin arrangement, in the conventional supercells, as visualized using VESTA[56] and shown in Figure 1. A conjugate gradient scheme was applied with the residual interatomic forces of 0.01 eV/Å acting on the atoms, and a self-consistent field convergence criterion better than 10^{-6} eV per unit cell was required. A Fermi smearing of 0.01 was considered in order to induce the total energy to absolute zero more accurately.[57] A plane-wave cutoff energy of 550 eV and a 4 × 4 × 2 Monkhorst−Pack[46] *k*-point mesh for the Brillouin zone sampling of a 1 × 1 × 1 unit-cell of $CuFeS_2$ were employed. It was suggested that the DFT + *U* methodology with the U_{eff} value of 5 eV is the most robust methodology to analyze the $CuFeS_2$ structure, which provides the best match to the experimental geometric properties, magnetic moment, and band gap values of $CuFeS_2$.[52]

In the present study, the DFT calculations have been performed with the same accuracy parameters applied in the previous study[52] and with the same value of plane-wave cutoff energy; however, the number of *k*-points has been adjusted related to the unit cell size. We have investigated different possible nonpolar terminations of $CuFeS_2(110)$. The slab modeled in the present work has lattice parameters as a = 10.418 Å and b = 7.443 Å. We tested different vacuum thicknesses and relaxed layer numbers to achieve the convergence within 1 meV per atom. Then, two layers of atoms at the base of the system were fixed with the same positions as their relaxed bulk positions. The surface were represented by one layer of atoms above these two layers and were permitted to move freely during the optimization. In addition, the vacuum region above the surface was at least 10 Å, which the results show that it is large enough to escape the interactions between the periodic slabs. The (1 × 1) surface cells consisting of 12 Cu, 12 Fe, and 24 S atoms have been sampled with a 3 × 5 × 1 Monkhorst−Pack[46] *k*-point mesh.

The surface energy of the relax slab has been calculated by considering both calculations of the relaxed and unrelaxed surfaces.[37,40] The top and bottom atomic layers of the surface are not the same after relaxation, and therefore it is required to take the unrelaxed surface energy (γ_u) into consideration to calculate the final surface energy of the relaxed surface. The unrelaxed surface energy is the surface energy before any surface optimization and is calculated as

$$\gamma_u = \frac{E_{slab,u} - nE_{bulk}}{2A} \quad (1)$$

where $E_{slab,u}$ is the energy of the unrelaxed slab; nE_{bulk} is the energy of an equal number of bulk atoms; and A is the surface area of one side of the slab. We calculated the relaxed surface energy (γ_r) from the total energy of the relaxed slab as follows

$$\gamma_r = \frac{E_{slab,r} - nE_{bulk}}{A} - \gamma_u \quad (2)$$

where $E_{slab,r}$ is the energy of the relaxed slab.

The adsorption energy of CO_2 molecule has been calculated by taking van der Waals interactions into account, which is crucial for the precise description of the interaction between CO_2 and a surface,[37,40] where the correction according to the Grimme method[58] for the long-range dispersion interactions (DFT-D2) has been applied. We have repeated few calculations to see the effect of dipole correction scheme; however, the results have shown that the difference in energy with and without the dipole correction here is less than 0.03 kJ/mol, which is not significant.

The interactions of the CO_2 adsorbate with the (110) $CuFeS_2$ surface slab have been modeled under conditions in which the atoms of the adsorbate and the first atomic layer of the slab have been allowed to relax without any constraint until residual forces on all atoms reached 0.01 eV/Å. In order to avoid periodic interactions between neighboring CO_2 molecules, the CO_2 adsorption has been calculated on a (1 × 2) supercell consisting of 24 Cu, 24 Fe, and 48 S atoms which has been sampled with a 5 × 3 × 1 Monkhorst−Pack[46] *k*-point mesh. Symmetry constraints have been excluded in the structural optimization; in particular, the CO_2 molecule can freely move in all directions and reorient until reaching the minimum energy adsorption structure. The isolated CO_2 molecule was also modeled in the center of a broken symmetry cell with lattice constants of 20 Å and was sampled by the γ-point of the Brillouin zone with the same accuracy parameters described for the surfaces.

The adsorption energy per molecule has been calculated as follows

$$E_{ads} = E_{surf+mol} - (E_{surf} + E_{mol}) \quad (3)$$

where $E_{surf+mol}$ is the total energy of the adsorbate−substrate system; E_{surf} is the energy of the surface slab; and E_{mol} is the energy of the isolated CO_2 molecule. Within this definition, the negative and positive values of adsorption energy would indicate an exothermic and endothermic process, respectively.

In order to elucidate the electronic properties and quantify the charge transfer between the surfaces and CO_2 molecule, a Bader charge analysis has been executed using the code developed by Henkelman and co-workers.[59,60]

3. RESULTS AND DISCUSSION

3.1. $CuFeS_2(110)$ Surface. Tasker[61] proposed a very simple model for surface stability of the ionic covalent compound by considering ionic crystal surfaces as stacks of planes, where three possibilities (type I, II, and III) can exist. In the type I surface, each plane has an overall zero charge because of the stoichiometric ratio of anions and cations that makes the surface nonpolar. Type II surfaces consist of charged layers but without a perpendicular charge because of stacking sequence, while type III surfaces have charged with the perpendicular dipole moment that causes the divergence of the surface energy with the size of the slab. According to Tasker,[61] in type I and II surfaces, the reconstruction of the surface is not needed because there is no net dipole perpendicular to the surface in the repeat unit. This causes the existence of these kinds of surfaces in nature with just small relaxation and reconstruction; however, type III surfaces require significant reconstruction in order to disperse the net charge. It is worth nothing that some surfaces of type I or II can also reconstruct considerably because of the important covalent character of the chalcopyrite. The reconstruction of (001), (100), (111), (112), (101), and (110) chalcopyrite surfaces was analyzed using DFT calculations within the plane-wave framework by de Oliveira et al.[59] In their study, only one termination for the (110) surface was introduced, while, in the present study, we investigate the (110) surface in detail, and three different possible terminations for the (110) surface have been obtained. In this section, these three possible terminations for the (110) surface (i.e., (110)_I, (110)_II, and (110)_III) and their surface energies have been presented. All the relaxed

DOI: 10.1021/acsomega.9b01988
ACS Omega XXXX, XXX, XXX−XXX

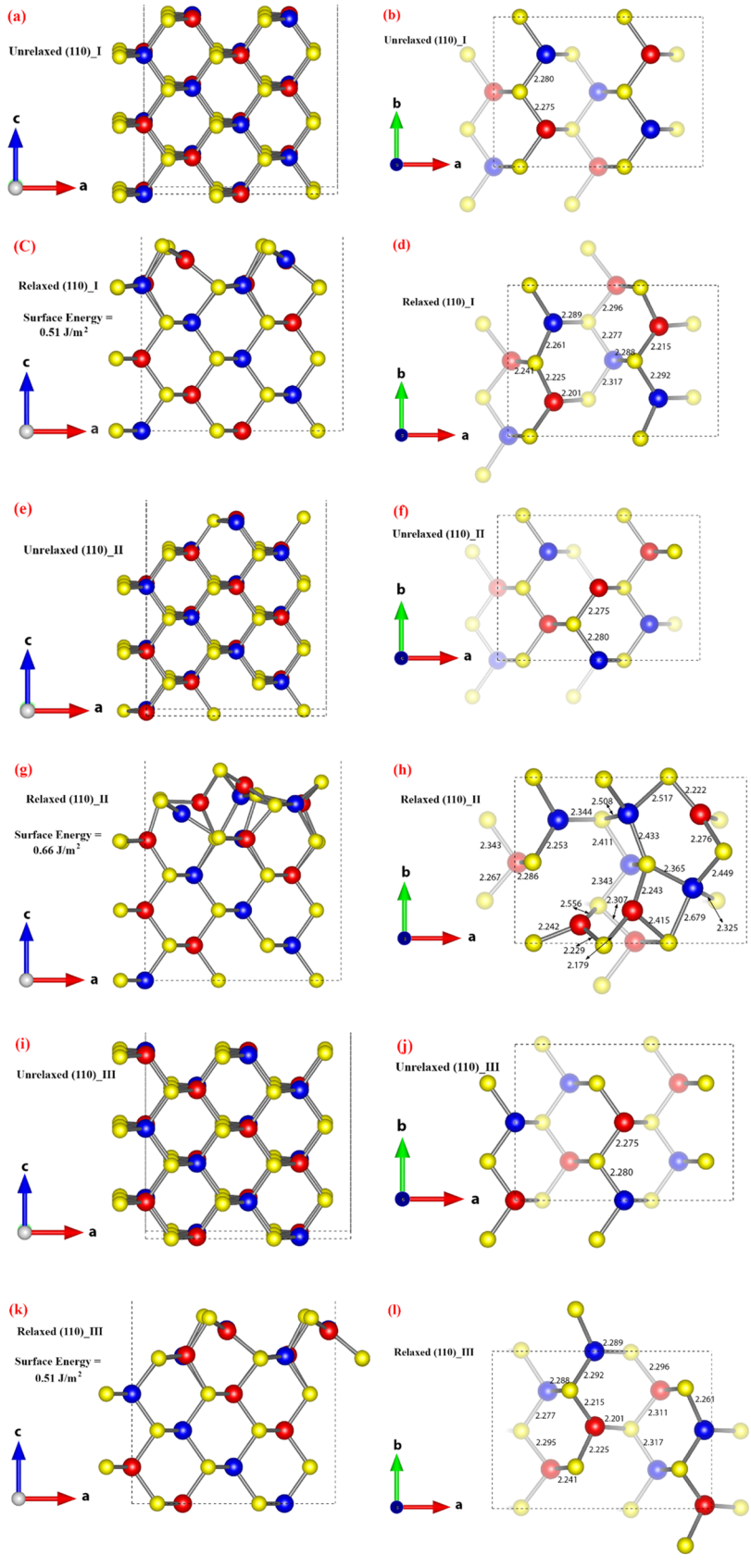

Figure 2. Unrelaxed and relaxed nonpolar (110) surfaces: (a)-(d) (110)_I, (e)-(h) (110)_II, and (i)-(l) (110)_III. Left panels show the side view of the (110) surface, while the top view of the (110) surface is shown in the right panels. Red, blue, and yellow spheres represent Cu, Fe, and S atoms, respectively. The S atoms are repeated in the edges because of the periodic boundary conditions.

DOI: 10.1021/acsomega.9b01988
ACS Omega XXXX, XXX, XXX−XXX

and unrelaxed structure of these three (110) surfaces are shown in Figure 2.

The unrelaxed (110) surface is a stepped surface with atomic layers composed by sulfur−metal−sulfur chains, as illustrated in Figure 2. The (110)_I and (110)_III $CuFeS_2$ surfaces do not reconstruct with the first atomic layer consisting of four sulfur, two iron, and two copper atoms, as shown in Figure 2a,b,i,j, respectively. In the present study, one reconstruction has been obtained for the $CuFeS_2$(110) surface, named the (110)_II surface. In the reconstructed (110)_II $CuFeS_2$ surface, half of the ions with the same charge from the first surface layer at the top of the repeated unit are removed and transferred to the bottom of the simulation slab. As a result, the surface obtained is partially vacant either in cations or onions so that the first atomic layer comprises two sulfur, one iron, and one copper atoms, as shown in Figure 2e,f. This configuration guarantees that the surface does not generate an electrical field within the crystal, and therefore the potential felt at each ion site reaches the constant bulk value.

After the relaxations of the two unreconstructed (110)_I and (110)_III surfaces, the metal Fe and Cu cations in the first atomic layer considerably relocate inward, while the surface S anions displace slightly outward toward the surface, as shown in Figure 2c,d,k,l. This displacement behavior of the surface atoms is consistent with the previously published computational studies.[21,62] This relaxation improves the metal−metal (Cu−Fe, Cu−Cu, and Fe−Fe) interactions in the first atomic layer and reduces under-coordination of surface cations. The Fe−S bond decreases from 2.280 to 2.261 Å, and the Cu−S bond decreases from 2.275 to around 2.225 Å. However, the relaxation of the reconstructed (110)_II surface which includes the half-vacant plane in the first atomic layer is found very unstable and there is no specific pattern for the surface layers, as shown in Figure 2g,h.

Once the surface with no dipole moment perpendicular to the surface is generated and relaxed, the surface energy is calculated using the relations 1 and 2. The surface energy of 0.51 J/m^2 is calculated for the two unreconstructed (110)_I and _III surfaces, which is in good agreement with the value of 0.58 J/m^2 calculated by Chen et al.,[21] while the slightly high value of 0.66 J/m^2 surface energy is calculated for the reconstructed (110)_II surface. Details are given in Table 1.

Table 1. Calculated surface energies of the $CuFeS_2$(110) Surfaces[a]

	(110)_I	(110)_II	(110)_III
current study	0.51	0.66	0.51
previous theoretical studies	0.58[21]	none	none

[a]The surface energies are in J/m^2.

3.2. CO_2 Adsorption on (110) Chalcopyrite Surfaces.

We studied the CO_2 adsorption by placing the molecule, parallelly and perpendicularly in different possible directions and exploring all possible atomic sites on a (1 × 2) supercell for all the surfaces obtained (Figure 3). During free relaxation, the CO_2 molecule prefers to move away from the surface, whilst remaining in a linear geometry, when placed parallel (*x*, *y*-directions) and perpendicular (*z*-direction) on the top of the first atomic layer of the surface. CO_2 is a linear molecule with two C═O bonds each with a length of 1.176 Å and a O−O bond with a length of 2.352 Å. To further investigate the interaction with atoms in the sublayer, we placed the molecule parallelly and perpendicularly close to different atomic sites in the second atomic layer in different possible directions. In contrast to the first atomic layer, the CO_2 molecule interacts with the surface and binds both exothermically and endothermally, when placed parallelly and perpendicularly to the surface in different adsorption configurations of the sublayer. We surprisingly notified the reactivity of the system with respect to CO_2 dissociation to form surface-bond CO and O species in a couple of configurations. CO_2 dissociation in all configurations is calculated to be endothermic with the energies of almost 100 kJ/mol. In this section, the results of the exothermal CO_2 adsorption onto the surface obtained are explained, and the results of the endothermal CO_2 adsorption are provided in the Supporting Information as Figures S1−S3.

3.2.1. $CuFeS_2$(110)_I Surface. The first set of CO_2 adsorption calculations was performed on the $CuFeS_2$(110)_I surface. The strongest binding was found, when we placed the molecule on top of the S atom in the subatomic layer bonded with the Fe_{suf1} atom in the top layer (Figure 3a), perpendicular to the surface in the *z*-direction (configuration A). In this configuration, the Fe_{suf1} atom in the top layer moves up by increasing the bonding with the S atom in the subatomic layer from 2.289 to 2.338 Å, whereas only one of the oxygen atoms, O_1, of the molecule binds at a surface Fe_{suf1} site [$d(Fe_{suf1}-O_1)$ = 2.315 Å], as shown in Figure 4a. As a result, the CO_2 molecule tilts relative to the surface normal and retaining a nearly linear structure with α(OCO) changing to 177.3°, whereas the C−O bonds slightly stretched to 1.181 and 1.169 Å for the two oxygen atoms O_1 and O_2, respectively. There is no other binding between the molecule and the surface, and we note that in this configuration, the CO_2 molecule binds exothermally to the $CuFeS_2$(110)_I surface with an adsorption energy of −22.8 kJ/mol.

The second strongest binding was found by placing the molecule perpendicular to the surface in the *z*-direction in the sublayer and in the middle of the space of the molecular ring, which contains of Fe_{suf1}, Cu_{suf2}, Cu_{sub1}, and three S atoms (configuration B) (Figure 3a). We found that, similar to configuration A, the Fe_{suf1} atom moves up while the bond length with the S atom in the second atomic layer decreases from 2.289 to 2.238 Å. Similar to configuration A, only one of the oxygen atoms, O_1, of the molecule binds at a surface Fe_{suf1} site [$d(Fe_{suf1}-O_1)$ = 2.255 Å], as shown in Figure 4b. The CO_2 molecule slightly bends to 177.4°, and the C−O bonds slightly stretched to 1.188 and 1.166 Å for the two oxygen atoms O_1 and O_2, respectively. The CO_2 adsorption to the $CuFeS_2$(110)_I surface is found to be −14.2 kJ/mol (exothermic adsorption).

The adsorption energies and representative parameters of these two configuration are summarized in Table 2. It shows that the most stable adsorption site is the Fe atom in the first atomic layer with an adsorption energy of −22.8 and −14.2 kJ/mol.

Different atomic sites of the $CuFeS_2$(110)_I surface were explored for possible interaction with the CO_2 molecule; however, only the two above configuration found to be exothermal adsorption energy, as presented above. The other configurations leading to endothermal adsorption energy are provided in the Supporting Information as Figure S1a−j.

Moreover, we also notice that for few initial placement of CO_2 molecules, the molecule dissociates into the CO and O species on the $CuFeS_2$(110)_I surface. In the first site (configuration C), the bond between the two nearby Fe_{sub1}

DOI: 10.1021/acsomega.9b01988
ACS Omega XXXX, XXX, XXX−XXX

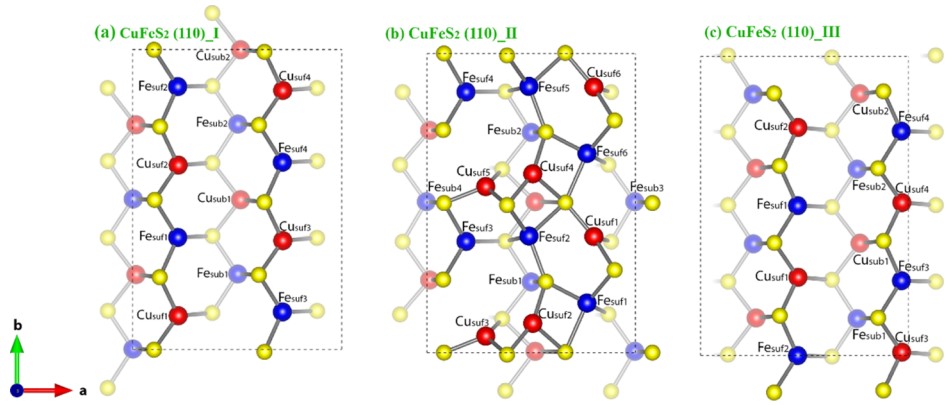

Figure 3. Top view of the (1 × 2) supercell of the relaxed (110) surfaces: (a) (110)_I, (b) (110)_II, and (c) (110)_III. Red, blue, and yellow spheres represent Cu, Fe, and S atoms, respectively. The S atoms are repeated in the edges because of the periodic boundary conditions.

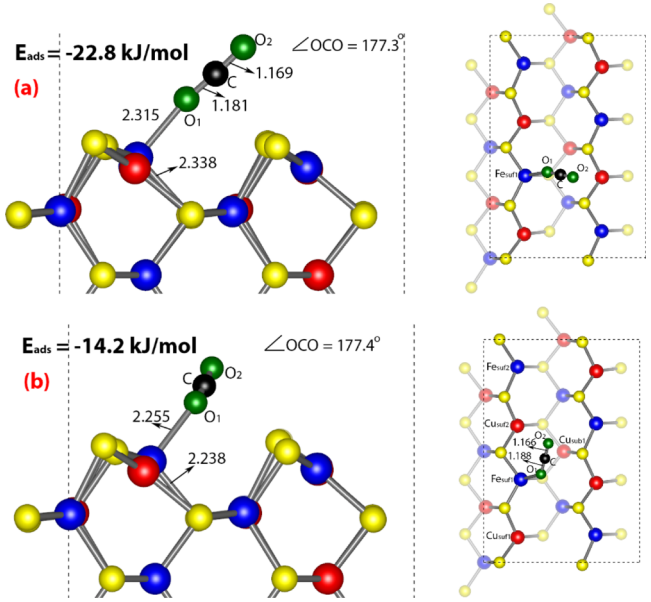

Figure 4. CO_2 molecule adsorbed on the (110)_I surface in (a) configuration A and (b) configuration B in a (1 × 2) supercell. Left panels illustrate the side views, while the top views are illustrated in the right panels. Red, blue, and yellow spheres represent Cu, Fe, and S surface atoms, respectively, while O and C atoms of the CO_2 molecule are represented by green and black spheres, respectively. Bond length values are in Angstroms.

and S atoms in the first atomic layer breaks, and the dissociated O atom of the CO_2 molecule, O_1, binds at the surface Fe_{suf1} site in the first atomic layer [$d(Fe_{suf1}-O_1)$ = 1.983 Å] and the Fe_{sub1} site in the second atomic layer [$d(Fe_{sub1}-O_1)$ = 2.059 Å] (Figure 5a). This dissociation of the CO_2 molecule is found, when the molecule is placed in the sublayer perpendicular to the surface in the *z*-direction and in an equal distance of the Fe_{suf1} and Cu_{suf1} atoms in the first atomic layer and close to the S atom made chain with both Fe_{suf1} and Cu_{suf1} atoms (Figure 3a). In addition, the bond between the two adjacent Cu_{suf1} and S atoms in the first atomic layer breaks, and the CO moiety with a bond length of 1.195 Å binds via the C atom at the adjacent Cu_{suf1} and S atoms [$d(Cu_{suf1}-C)$ = 1.995 Å and $d(S-C)$ = 1.719 Å].

The second site (configuration D) leading to the CO_2 molecule dissociation is, when the CO_2 molecule is placed in the sublayer perpendicular to the surface in the *z*-direction in an equal distance of the Fe_{suf1} and Cu_{suf2} atoms in the first atomic layer and close to the S atom bonded with both Fe_{suf1} and Cu_{suf2} atoms (Figure 3a). In this configuration, the dissociated O species, O_1, binds at a site between two adjacent surface Fe_{suf1} site [$d(Fe_{suf1}-O_1)$ = 1.869 Å] and the S atom in the second atomic layer [$d(S-O_1)$ = 1.594 Å] (Figure 5b). In addition, similar to configuration C, the bond between the two adjacent Cu_{suf2} and S atoms in the first atomic layer breaks, and the CO moiety binds via the C atom at the adjacent Cu_{suf2} and S atoms [$d(Cu_{suf2}-C)$ = 1.986 Å and $d(S-C)$ = 1.763 Å] with a bond length of 1.191 Å. These results for both configuration C and configuration D show that spontaneous dissociation of the CO_2 molecule is possible over the $CuFeS_2$(110)_I surface through interaction of the CO_2 molecule with sublayer surface atoms.

3.2.2. $CuFeS_2$(110)_II Surface. As described earlier, there is no specific pattern in the reconstructed (110)_II surface (Figure 2g,h), while different possible sites of the surface are considered to study the CO_2 adsorption by placing the molecule on these sites in different directions. The strongest binding is found by placing the CO_2 molecule perpendicular to the surface in the *z*-direction in the sublayer in the middle of the space of the molecular ring obtained, which contains the Fe_{suf1}, Cu_{suf1}, Fe_{suf2}, and three S atoms (configuration A) (Figure 3b). We note that the bonds between the S atom and two nearby Fe_{suf2} in the first atomic layer and Fe_{sub1} atoms in the second atomic layer break, whereas the CO_2 molecule binds via the O_2 atom at the Fe_{suf2} atom [$d(Fe_{suf2}-O_2)$ = 2.008 Å] and also binds via the C atom at the S atom [$d(C-S)$ = 1.771 Å] (Figure 6a). In addition, the other O atom, O_1, binds at both Fe_{suf1} atom [$d(Fe_{suf1}-O_1)$ = 2.198 Å] and Fe_{sub1} [$d(Fe_{sub1}-O_1)$ = 2.076 Å]. As a result, the molecule loses linearity [α(OCO) = 124.1°], and the two C−O_1 and C−O_2

Table 2. CO_2 Adsorption Energies and Representative Parameters for the $CuFeS_2$(110)_I Surface

adsorption site	bonding type	E_{ads} (kJ/mol)	$d(C-O_1)$ (Å)	$d(C-O_2)$ (Å)	α(OCO) (deg)	$d(Fe-O_1)$ (Å)	figures
Fe_{suf1}	config. A	−22.8	1.181	1.169	177.3	2.315	3a
Fe_{suf1}	config. B	−14.2	1.188	1.166	177.4	2.255	3b

DOI: 10.1021/acsomega.9b01988
ACS Omega XXXX, XXX, XXX−XXX

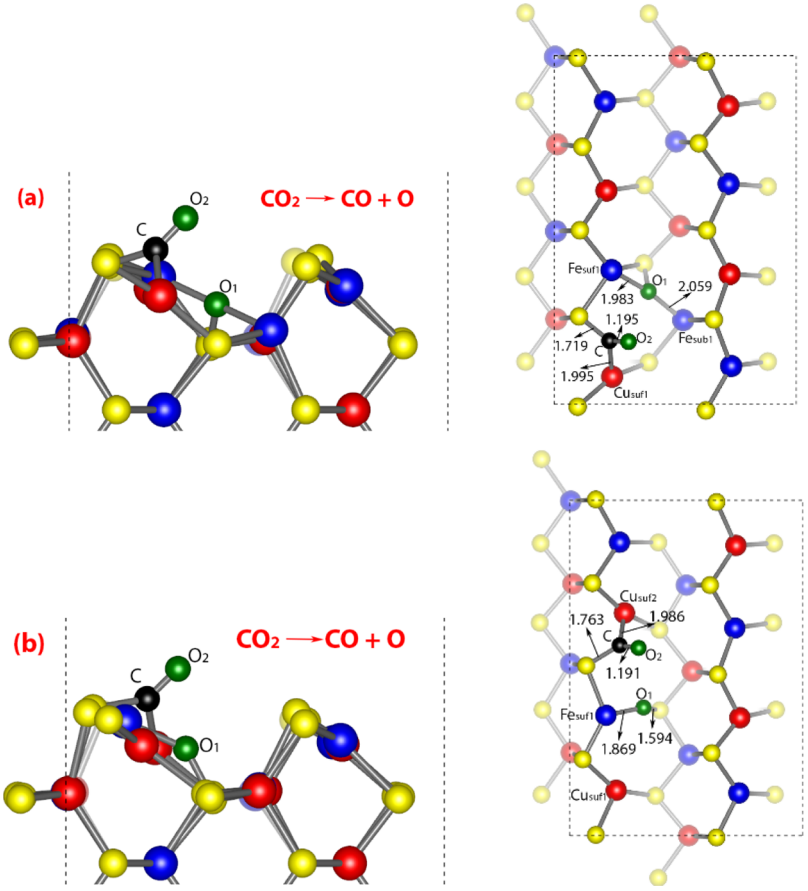

Figure 5. Spontaneous dissociation of the CO_2 molecule into the CO molecule on the (110)_I surface in (a) configuration C and (b) configuration D in a (1 × 2) supercell. Left panels illustrate the side views, while the top views are illustrated in the right panels. Red, blue, and yellow spheres represent Cu, Fe, and S surface atoms, respectively, while O and C atoms of the CO_2 and CO molecules are represented by green and black spheres, respectively.

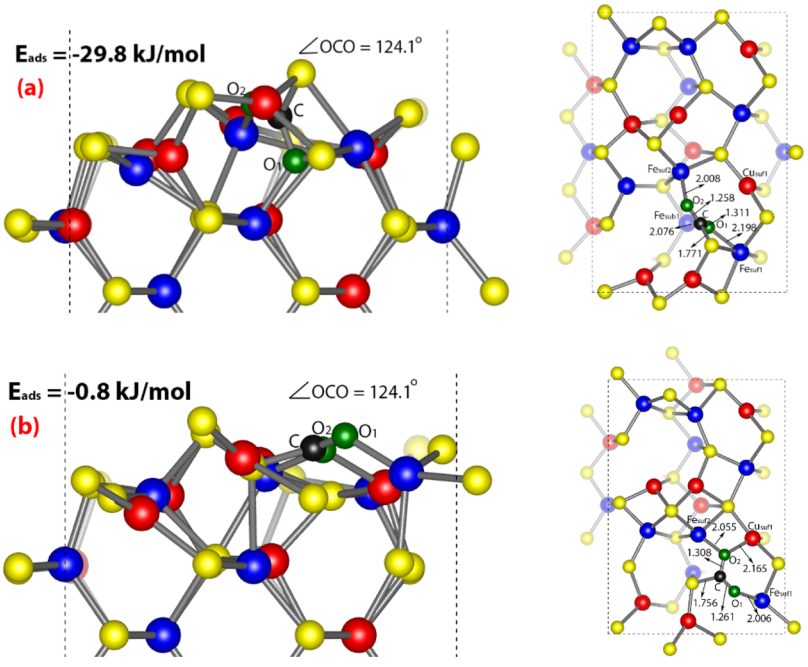

Figure 6. CO_2 molecule adsorbed on the (110)_II surface in (a) configuration A and (b) configuration B in a (1 × 2) supercell. Left panels illustrate the side views, while the top views are illustrated in the right panels. Red, blue, and yellow spheres represent Cu, Fe, and S surface atoms, respectively, while O and C atoms of the CO_2 molecule are represented by green and black spheres, respectively. Bond length values are in Angstroms.

DOI: 10.1021/acsomega.9b01988
ACS Omega XXXX, XXX, XXX−XXX

Table 3. CO_2 Adsorption Energies and Representative Parameters for the $CuFeS_2(110)$_II Surface

adsorption sites	bonding type	E_{ads} (kJ/mol)	d(C−O_1) (Å)	d(C−O_2) (Å)	α(OCO) (deg)	d(C−S) (Å)	figures
{O_1: (Fe_{suf1}; Fe_{sub})} {O_2: (Fe_{suf2})} {C: (S)}	config. A	−29.8	1.311	1.258	124.1	1.771	5a
{O_1: (Fe_{suf1})} {O_2: (Fe_{suf2}; Cu_{suf1})} {C: (S)}	config. B	−0.8	1.261	1.308	124.1	1.756	5b

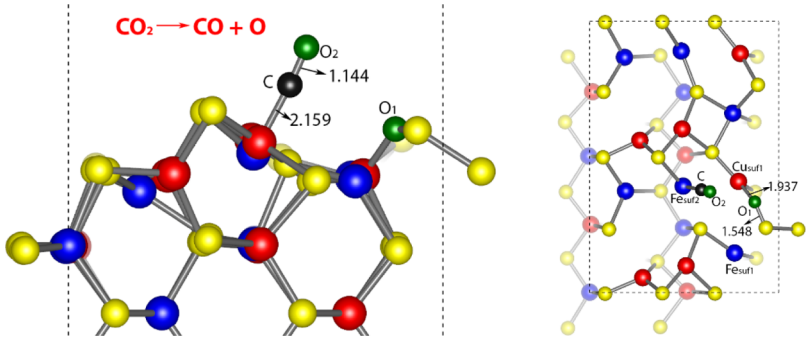

Figure 7. CO_2 molecule dissociation to the CO molecule on the (110)_II surface in configuration C in a (1 × 2) supercell. The left panel illustrates the side view, while the top view is illustrated in the right panel. Red, blue, and yellow spheres represent Cu, Fe, and S surface atoms, respectively, while O and C atoms of the CO_2 and CO molecules are represented by green and black spheres, respectively.

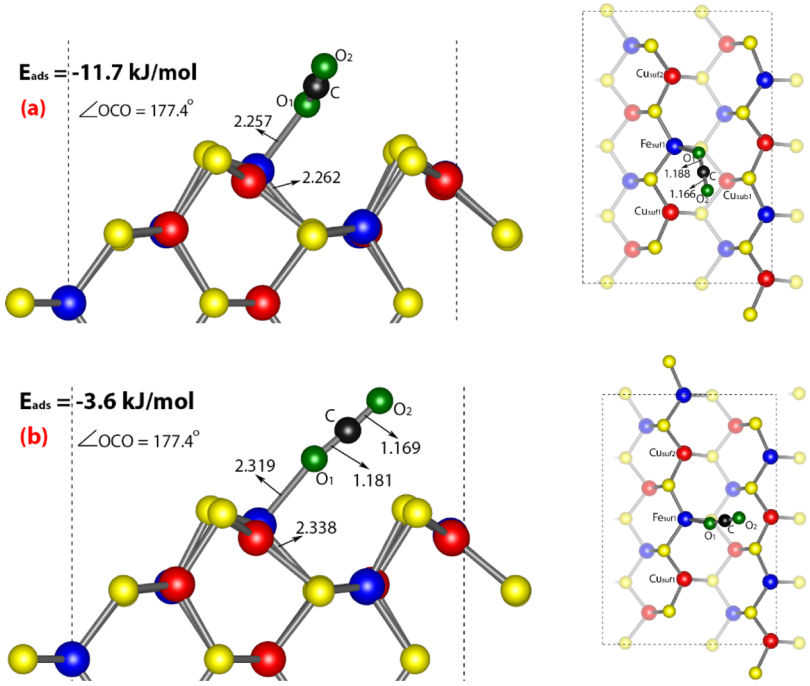

Figure 8. CO_2 molecule adsorbed on the (110)_III surface in (a) configuration A and (b) configuration B in a (1 × 2) supercell. Left panels illustrate the side views, while the top views are illustrated in the right panels. Red, blue, and yellow spheres represent Cu, Fe, and S surface atoms, respectively, while O and C atoms of the CO_2 molecule are represented by green and black spheres, respectively. Bond length values are in angstroms.

bonds are elongated to 1.311 and 1.258 Å, respectively. In this configuration, the CO_2 molecule adsorbs exothermally with an adsorption energy of −29.8 kJ/mol.

The CO_2 molecule also binds exothermally to the surface in a different configuration (configuration B) with a binding energy of −0.8 kJ/mol, when placed in the same site as configuration A but parallel to the surface in the y-direction. Here also, the bonds between the S atom and two Fe_{suf1} and Fe_{suf2} atoms in the first atomic layer break, whereas the CO_2 molecule binds via the O_1 atom at the Fe_{suf1} atom [d(Fe_{suf1}−O_1) = 2.006 Å] and also binds through the C atom at the S atom [d(C−S) = 1.756 Å] (Figure 6b). In addition, the other O atom, O_2, binds at both Fe_{suf2} atom [d(Fe_{suf2}−O_2) = 2.055 Å] and Cu_{suf1} in the first atomic layer [d(Cu_{suf1}−O_2) = 2.165 Å]. As a result, the CO_2 molecule loses linearity to change α(OCO) to 124.1°, and the two C−O_1 and C−O_2 bonds are lengthened to 1.261 and 1.308 Å, respectively.

The adsorption energies and representative parameters of these two configuration are summarized in Table 3. It shows that the most stable adsorption sites for the oxygen atoms are the Fe atom in the first and second atomic layers, similar to the $CuFeS_2(110)$_I, and the S atom is the strongest bonding site for the C atom with an adsorption energy of −29.8 and −0.8 kJ/mol.

Here, only the above two configurations are found to be exothermal adsorption energy on the $CuFeS_2(110)$_II surface,

DOI: 10.1021/acsomega.9b01988
ACS Omega XXXX, XXX, XXX−XXX

Table 4. CO_2 Adsorption Energies and Representative Parameters for the $CuFeS_2(110)\_I$ Surface

adsorption site	bonding type	E_{ads} (kJ/mol)	$d(C-O_1)$ (Å)	$d(C-O_2)$ (Å)	$\alpha(OCO)$ (deg)	$d(Fe-O_1)$ (Å)	figures
Fe_{suf1}	config. A	−11.7	1.188	1.166	177.4	2.257	7a
Fe_{suf1}	config. B	−3.6	1.181	1.169	177.4	2.319	7b

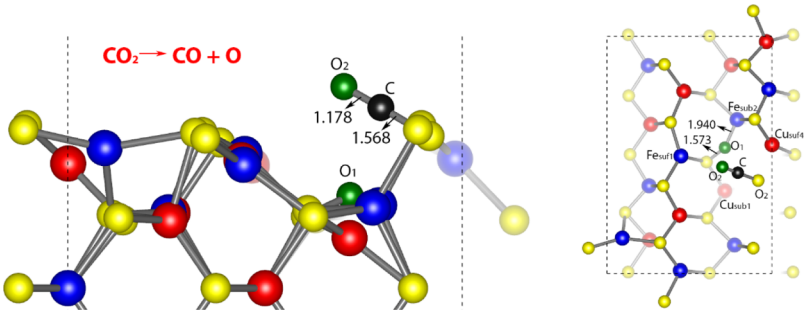

Figure 9. CO_2 molecule dissociation to the CO molecule on the (110)_III surface in configuration C in a (1 × 2) supercell. The left panel illustrates the side view, while the top view is illustrated in the right panel. Red, blue, and yellow spheres represent Cu, Fe, and S surface atoms, respectively, while O and C atoms of the CO_2 and CO molecules are represented by green and black spheres, respectively.

and the other configurations leading to endothermal adsorption energy are provided in the Supporting Information as Figure S2a−g.

Similar to the $CuFeS_2(110)\_I$ surface, the CO_2 molecule dissociation to the CO and O species was also observed here on the $CuFeS_2(110)\_II$ surface but only for one initial configuration among different possible configurations investigated. In this configuration, the bonds between two adjacent Fe_{suf2} and S atoms as well as Cu_{suf1} and its nearby S atom in the first atomic layer break, when the CO_2 molecule is placed in the same site as configuration A but parallel to the surface in the *x*-direction (configuration C). The CO moiety binds via the C atom with the Fe_{suf2} atom [$d(Fe_{suf2}-C)$ = 2.159 Å] having a bond length of 1.144 Å, in which the Fe_{suf2} atom bond with the adjacent S atom is broken. In addition, the dissociated O species, O_1, binds at the bridge site between two adjacent surface Cu_{suf1} [$d(Cu_{suf1}-O_1)$ = 1.937 Å] and the S atoms in the first atomic layer [$d(S-O_1)$ = 1.548 Å] (Figure 7).

3.2.3. $CuFeS_2(110)\_III$ Surface. As described earlier, the relaxed $CuFeS_2(110)\_III$ surface is a stable surface similar to the $CuFeS_2(110)\_I$ surface with the same energy surface of 0.51 J/m^2. In this surface, Fe and Cu atoms in the first atomic layer significantly displace inward toward the bulk, while the surface S atoms relocate slightly outward toward the surface (Figure 2k,l). We found similar adsorption sites on this surface, while the CO_2 molecule binds with different adsorption energy values.

The CO_2 molecule binds weakly in exothermic fashion (−11.7 kJ/mol) on this surface on placing it parallel to the surface in the *y*-direction in the sublayer in the middle of the space of the molecular ring, consisting of the Fe_{suf1}, Cu_{suf1}, Cu_{sub1}, and three S atoms (configuration A) (Figure 3c). In this configuration, the molecule binds at a surface Fe_{suf1} site through only one of its oxygen atoms, O_1, [$d(Fe_{suf1}-O_1)$ = 2.257 Å], as shown in Figure 8a. We note that the Fe_{suf1} atom moves slightly upward while the bonding with the S atom in the second atomic layer decreases from 2.289 to 2.262 Å. As a result, the CO_2 molecule holding nearly its linear structure with $\alpha(OCO)$ changing to 177.4° and skewed relative to the surface normal, whereas the C−O bonds are slightly stretched to 1.188 and 1.166 Å for the two oxygen atoms O_1 and O_2, respectively.

We found another exothermic adsorption configuration by placing the molecule perpendicular to the surface in the *z*-direction on top of the S atom in the second atomic layer, which has a bond with the Fe_{suf1} atom in the first atomic layer (configuration B) (Figure 3a). We found that, similar to configuration A, the Fe_{suf1} atom moves up by increasing the bonding with the S atom in the second atomic layer from 2.289 to 2.338 Å, whereas only one of the oxygen atoms, O_1, of the molecule binds at a surface Fe_{suf1} site [$d(Fe_{suf1}-O_1)$ = 2.319 Å], as shown in Figure 8b. We note that the CO_2 molecule slightly loses the linearity and bends to 177.4°, and the C−O bonds are slightly stretched to 1.181 and 1.169 Å for the two oxygen atoms O_1 and O_2, respectively. The CO_2 adsorbs exothermally to the surface with an adsorption energy of −3.6 kJ/mol.

The adsorption energies and representative parameters of these two configuration are summarized in Table 4. Similar to the $SuFeS_2(110)\_I$ surface, it shows that the most stable adsorption site on the $SuFeS_2(110)\_III$ surface is the Fe atom in the first atomic layer, but the CO_2 molecule adsorbs weaker on this surface than the $SuFeS_2(110)\_I$ surface with the adsorption energy of −11.7 and −3.6 kJ/mol.

All other possible sites of the surface were explored to study the CO_2 adsorption on the surface, and the other configuration leading to endothermic adsorption energy is provided in the Supporting Information as Figure S3a−j.

Similar to the two surfaces described above, the CO_2 molecule dissociation to the CO and O species was also found on the $CuFeS_2(110)\_III$ surface. The molecule dissociated when we placed it perpendicular to the surface in the *z*-direction in the sublayer in the middle of the space of the molecular ring, which contains the Cu_{suf4}, Cu_{sub1}, Fe_{sub2}, and three S atoms (configuration C) (Figure 3c). We also note that the molecule dissociates similar to the configuration C by placing it near the Cu_{suf4} in the same molecular ring. In both configuration, the bonds between the Fe_{sub2} and the adjacent lower S atom break and the dissociated O species, O_1, binds at the Fe_{sub2} [$d(Fe_{sub2}-O_1)$ = 1.940 Å] and S atoms [$d(S-O_1)$ = 1.573 Å] (Figure 9). The CO moiety with a bond length of 1.178 Å binds through the C atom at the S atom in the first atomic layer [$d(S-C)$ = 1.568 Å], which its bonds with two adjacent Cu atoms are broken.

DOI: 10.1021/acsomega.9b01988
ACS Omega XXXX, XXX, XXX−XXX

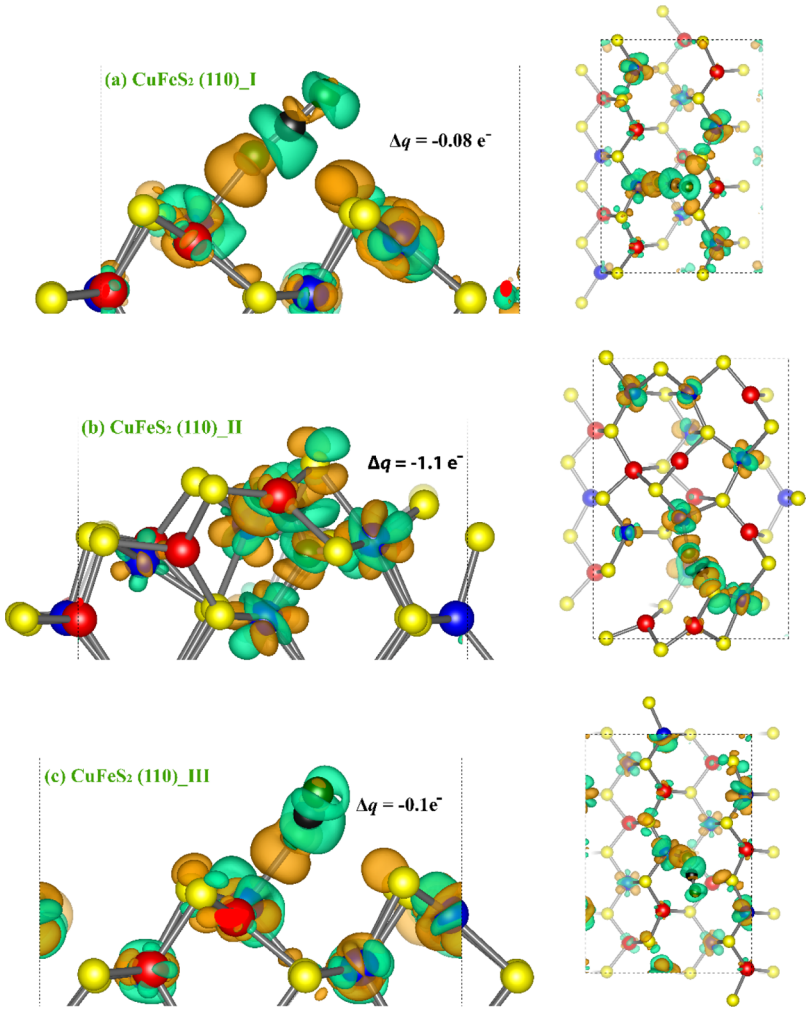

Figure 10. Electronic density difference plot of CO_2 adsorption structures on (a) $CuFeS_2(110)$_I, (b) $CuFeS_2(110)$_II, and (c) $CuFeS_2(110)$_III surfaces in the most stable exothermic configurations, showing charge transfer in the regions between the CO_2 and the atoms in the first atomic layer. The left panel illustrates the side view, while the top view is illustrated in the right panel. Orange contours indicate the electron density increases by 0.02 electrons/Å^3, and green contours indicate the electron density decreases by 0.02 electrons/Å^3.

3.3. Electronic Charge Transfer Analysis. Because the CO_2 molecule may receive electrons into its lowest unoccupied molecular orbital to form a negatively charged bent species ($CO_2^{-\delta}$), we have quantified the electron transfer from the surface to the CO_2 molecule by performing Bader charge analysis on the most exothermic $CuFeS_2$–CO_2 adsorption configurations on all three surfaces (Figures 4a, 6a, and 8a). A clear charge transfer from the surfaces to the adsorbed CO_2 molecule has been observed calculated through the difference of the charges on the CO_2 molecule [$\Delta q(CO_2)$] in the adsorption configurations to the isolated CO_2 molecule. We note that the charge transfer is more prominent in the most exothermic adsorption configuration on the $CuFeS_2(110)$_II (Figure 6a), where a net charge of 1.10 e$^-$ is transferred to the adsorbed CO_2 molecule. In the most exothermic adsorption configurations on the $CuFeS_2(110)$_I (Figure 4a) and $CuFeS_2(110)$_III (Figure 8a); however, the CO_2 molecule gained a net charge of 0.08 and 0.10 e$^-$, respectively, from the surface species. We plotted the electronic charge density difference in order to originate further insight into local charge rearrangement of the surfaces because of the CO_2 adsorption. The electronic charge density difference can be obtained by subtracting from the charge density of the total adsorbate–substrate system, the sum of the charge densities of the CO_2 molecule, and the clean $CuFeS_2(110)$ surfaces, calculated using the same geometry as the adsorbate–substrate system. Shown in Figure 10 are the electron density difference isosurface plots, illustrating the electron redistribution within the CO_2–$CuFeS_2$ systems. We observe that the adsorbed CO_2 molecule is activated with a net negative charge and is localized on the oxygen atoms binded to the surfaces. As noted, we observed a significant structural change in the CO_2 molecule as a result of its activation, changing from a neutral linear molecule to a negatively charged ($CO_2^{-\delta}$) slightly or considerably bent species, with elongated C–O bond distances (Tables 1, 2, and 3).

4. CONCLUSIONS

We have used the DFT + U methodology to describe $CuFeS_2$ surface structures and presented the analyses of the CO_2 adsorption and activation on the $CuFeS_2(110)$ surfaces. Plane-wave density functional calculations have been applied to study the reconstruction of the (110) $CuFeS_2$ surfaces. Three possible stable surface terminations for the (110) surface have been proposed, and reconstruction has been explained in detail.

DOI: 10.1021/acsomega.9b01988
ACS Omega XXXX, XXX, XXX–XXX

Among three different surface configurations, the two terminations are found to be more stable, and for these surface terminations, we found that the most stable site for adsorption is the iron atom binded to one of the oxygen atoms with an adsorption energy equal to ∼−22.8 and −11.7 kJ/mol, whereas the CO_2 molecule holding nearly its linear structure and skewed relative to the surface normal, and the C−O bonds are elongated for the two oxygen atoms. However, the other (110) surface exhibits stronger adsorption (∼−29.8 kJ/mol), and the most stable site for adsorption is the iron atom binded to the oxygen atoms and the sulfur atom binded to the carbon atom, whereas the molecule loses linearity, and the two C−O bonds are also elongated. We also notice spontaneous dissociation of the CO_2 molecule into CO and O species on all the three surfaces, where one of the oxygen atoms binds with two surface atoms in the first and second atomic layer.

We note that the CO_2 molecule accepts electrons into its lowest unoccupied molecular orbital to form a negatively charged species on the surfaces as confirmed by Bader charge analysis, and the structure of the surface plays a significant role in the activation of CO_2. Elongation of the C−O bonds is observed in the adsorbed molecule on these surfaces compared to the gas-phase molecule, showing activation of the CO_2 molecule over these surfaces. Future work will include investigations of reaction pathways for the CO_2 conversion on the different surfaces of $CuFeS_2$. Catalytic processes are extremely complex in nature because of occurring in a multicomponent environment, and various environmental parameters such as temperature, pressure, and electrode potential could affect the process. However, DFT calculations at 0 K, as presented in this paper, would provide mechanistic insight into CO_2 activation on the (110) $CuFeS_2$ surface, and this fundamental understanding would still be relevant for applications at higher temperatures.

■ ASSOCIATED CONTENT

Supporting Information

The Supporting Information is available free of charge on the ACS Publications website at DOI: 10.1021/acsomega.9b01988.

Sites of the surfaces to study the CO_2 adsorption leading to endothermic adsorption energy for $CuFeS_2$(110)_I, $CuFeS_2$(110)_II, and $CuFeS_2$(110)_III (PDF)

■ AUTHOR INFORMATION

Corresponding Authors

*E-mail: rasoul.khaledialidusti@ntnu.no (R.K.).
*E-mail: akmishra@ddn.upes.ac.in, mishra_lu@hotmail.com (A.K.M.).
*E-mail: afrooz.barnoush@ntnu.no (A.B.).

ORCID

Rasoul Khaledialidusti: 0000-0002-7604-1699

Notes

The authors declare no competing financial interest.

■ ACKNOWLEDGMENTS

The authors would like to acknowledge and greatly appreciate financial support from VISTA, which is a basic research program in collaboration between the Norwegian Academy of Science and Letters, and Statoil. The authors would also like to thank the Department of Mechanical and Industrial Engineering at Norwegian University of Science and Technology (NTNU). The authors also acknowledge generous grants of high-performance computer time from both Vilje and UNINETT Sigma.

■ REFERENCES

(1) Hulliger, F. Crystal chemistry of the chalcogenides and pnictides of the transition elements. *Structure and Bonding*; Springer: Berlin, Heidelberg, 1968; pp 83−229.
(2) Pearce, C. I.; Pattrick, R. A. D.; Vaughan, D. J.; Henderson, C. M. B.; Van der Laan, G. Copper oxidation state in chalcopyrite: Mixed Cu d9 and d10 characteristics. *Geochim. Cosmochim. Acta* **2006**, *70*, 4635−4642.
(3) Von Oertzen, G. U.; Harmer, S. L.; Skinner, W. M. XPS andab initiocalculation of surface states of sulfide minerals: pyrite, chalcopyrite and molybdenite. *Mol. Simul.* **2006**, *32*, 1207−1212.
(4) Shay, J. L.; Wernick, J. H. *The science of the solid State*; Program Press: New York, 1975; Vol. 7.
(5) Migliorato, P.; Tell, B.; Shay, J. L.; Kasper, H. M. Junction electroluminescence in $CuInSe_2$. *Appl. Phys. Lett.* **1974**, *24*, 227−228.
(6) Zhao, Y.-J.; Mahadevan, P.; Zunger, A. Comparison of predicted ferromagnetic tendencies of Mn substituting the Ga site in III-V's and in I-III-VI2 chalcopyrite semiconductors. *Appl. Phys. Lett.* **2004**, *84*, 3753−3755.
(7) Marrón, D. F.; Martí, A.; Luque, A. Thin-film intermediate band chalcopyrite solar cells. *Thin Solid Films* **2009**, *517*, 2452−2454.
(8) Árnadóttir, L.; Stuve, E. M.; Jónsson, H. Adsorption of water monomer and clusters on platinum(111) terrace and related steps and kinks. *Surf. Sci.* **2010**, *604*, 1978−1986.
(9) Erdogan, R.; Ozbek, O.; Onal, I. A periodic DFT study of water and ammonia adsorption on anatase TiO_2 (001) slab. *Surf. Sci.* **2010**, *604*, 1029−1033.
(10) Hejduk, P.; Szaleniec, M.; Witko, M. Molecular and dissociative adsorption of water at low-index V_2O_5 surfaces: DFT studies using cluster surface models. *J. Mol. Catal. A: Chem.* **2010**, *325*, 98−104.
(11) Ivaništšev, V.; Nazmutdinov, R. R.; Lust, E. Density functional theory study of the water adsorption at Bi (111) electrode surface. *Surf. Sci.* **2010**, *604*, 1919−1927.
(12) Zhang, Z. W.; Li, J. C.; Jiang, Q. Hydrogen adsorption on Eu/SWCNT systems: a DFT study. *J. Phys. Chem. C* **2010**, *114*, 7733−7737.
(13) Stirling, A.; Bernasconi, M.; Parrinello, M. Ab initio simulation of H_2S adsorption on the (100) surface of pyrite. *J. Chem. Phys.* **2003**, *119*, 4934−4939.
(14) Stirling, A.; Bernasconi, M.; Parrinello, M. Ab initiosimulation of water interaction with the (100) surface of pyrite. *J. Chem. Phys.* **2003**, *118*, 8917−8926.
(15) de Lima, G. F.; de Oliveira, C.; de Abreu, H. A.; Duarte, H. A. Water adsorption on the reconstructed (001) chalcopyrite surfaces. *J. Phys. Chem. C* **2011**, *115*, 10709−10717.
(16) de Lima, G. F.; de Oliveira, C.; de Abreu, H. A.; Duarte, H. A. Sulfuric and hydrochloric acid adsorption on the reconstructed sulfur terminated (001) chalcopyrite surface. *Int. J. Quantum Chem.* **2012**, *112*, 3216−3222.
(17) Nørskov, J. K.; Bligaard, T.; Rossmeisl, J.; Christensen, C. H. Towards the computational design of solid catalysts. *Nat. Chem.* **2009**, *1*, 37.
(18) Harmer, S. L.; Pratt, A. R.; Nesbitt, W. H.; Fleet, M. E. Sulfur species at chalcopyrite ($CuFeS_2$) fracture surfaces. *Am. Mineral.* **2004**, *89*, 1026−1032.
(19) Barkat, L.; Hamdadou, N.; Morsli, M.; Khelil, A.; Bernède, J. C. Growth and characterization of $CuFeS_2$ thin films. *J. Cryst. Growth* **2006**, *297*, 426−431.
(20) Shukri, Z. A.; Champness, C. H. Cleavage and Twinning in CuInSe2Crystals. *Acta Crystallogr., Sect. B: Struct. Crystallogr. Cryst. Chem.* **1997**, *53*, 620.
(21) Chen, V. H.-Y.; Mallia, G.; Martínez-Casado, R.; Harrison, N. M. Surface morphology of $CuFeS_2$: The stability of the polar (112)/

DOI: 10.1021/acsomega.9b01988
ACS Omega XXXX, XXX, XXX−XXX

(11$\bar{2}$) surface pair. *Phys. Rev. B: Condens. Matter Mater. Phys.* **2015**, *92*, 155426.
(22) Mönch, W. *Semiconductor Surfaces and Interfaces*. Springer Series in Surface Science; springer verlag berlin heidelberg, 1995; Vol. *26*.
(23) Lannoo, M.; Friedel, P. *Atomic and Electronic Structure of Surfaces*. Springer Series in Surface Science; springer verlag berlin heidelberg, 1991; Vol. *16*.
(24) Chandraprabha, M. N.; Natarajan, K. A. Surface chemical and flotation behaviour of chalcopyrite and pyrite in the presence of Acidithiobacillus thiooxidans. *Hydrometallurgy* **2006**, *83*, 146−152.
(25) Nasluzov, V.; Shor, A.; Romanchenko, A.; Tomashevich, Y.; Mikhlin, Y. DFT+ U and Low-Temperature XPS Studies of Fe-Depleted Chalcopyrite ($CuFeS_2$) Surfaces: A Focus on Polysulfide Species. *J. Phys. Chem. C* **2019**, *123*, 21031.
(26) Huaman, R. N. E.; Jun, T. X. Energy related CO_2 emissions and the progress on CCS projects: a review. *Renew. Sustain. Energy Rev.* **2014**, *31*, 368−385.
(27) Centi, G.; Perathoner, S. Catalysis: role and challenges for a sustainable energy. *Top. Catal.* **2009**, *52*, 948−961.
(28) Roy, S. C.; Varghese, O. K.; Paulose, M.; Grimes, C. A. Toward solar fuels: photocatalytic conversion of carbon dioxide to hydrocarbons. *ACS Nano* **2010**, *4*, 1259−1278.
(29) Valenzano, L.; Civalleri, B.; Chavan, S.; Palomino, G. T.; Areán, C. O.; Bordiga, S. Computational and Experimental Studies on the Adsorption of CO, N_2, and CO_2 on Mg-MOF-74. *J. Phys. Chem. C* **2010**, *114*, 11185−11191.
(30) Poloni, R.; Smit, B.; Neaton, J. B. CO_2 capture by metal−organic frameworks with van der Waals density functionals. *J. Phys. Chem. A* **2012**, *116*, 4957−4964.
(31) Poloni, R.; Lee, K.; Berger, R. F.; Smit, B.; Neaton, J. B. Understanding trends in CO_2 adsorption in metal−organic frameworks with open-metal sites. *J. Phys. Chem. Lett.* **2014**, *5*, 861−865.
(32) McDonald, T. M.; Mason, J. A.; Kong, X.; Bloch, E. D.; Gygi, D.; Dani, A. Cooperative insertion of CO_2 in diamine-appended metal-organic frameworks. *Nature* **2015**, *519*, 303.
(33) Isaacs, M.; Canales, J. C.; Aguirre, M. J.; Estiú, G.; Caruso, F.; Ferraudi, G.; Costamagna, J. Electrocatalytic reduction of CO_2 by azamacrocyclic complexes of Ni(II), Co(II), and Cu(II). Theoretical contribution to probable mechanisms. *Inorg. Chim. Acta* **2002**, *339*, 224−232.
(34) Darensbourg, D. J. Making plastics from carbon dioxide: salen metal complexes as catalysts for the production of polycarbonates from epoxides and CO_2. *Chem. Rev.* **2007**, *107*, 2388−2410.
(35) Yan, T.; Wang, S.; Zhou, Y.; Cao, Z.; Li, G. Adsorption of CO_2 on the rutile (110) surface in ionic liquid. A molecular dynamics simulation. *J. Phys. Chem. C* **2009**, *113*, 19389−19392.
(36) Li, S. F.; Guo, Z. X. CO_2 activation and total reduction on titanium (0001) surface. *J. Phys. Chem. C* **2010**, *114*, 11456−11459.
(37) Mishra, A. K.; Roldan, A.; de Leeuw, N. H. CuO surfaces and CO_2 activation: a dispersion-corrected DFT+ U study. *J. Phys. Chem. C* **2016**, *120*, 2198−2214.
(38) Mishra, A. K.; Roldan, A.; de Leeuw, N. H. A density functional theory study of the adsorption behaviour of CO_2 on Cu_2O surfaces. *J. Chem. Phys.* **2016**, *145*, 044709.
(39) Mishra, A. K.; de Leeuw, N. H. Mechanistic insights into the Cu (I) oxide-catalyzed conversion of CO_2 to fuels and chemicals: A DFT approach. *J. CO2 Util.* **2016**, *15*, 96−106.
(40) Khalediali dusti, R.; Mishra, A. K.; Barnoush, A. Rheological properties of super critical CO_2 with CuO: Multi-scale computational modeling. *J. Chem. Phys.* **2018**, *149*, 224702.
(41) Yu, X.; Zhang, X.; Jin, L.; Feng, G. CO adsorption, oxidation and carbonate formation mechanisms on Fe_3O_4 surfaces. *Phys. Chem. Chem. Phys.* **2017**, *19*, 17287−17299.
(42) Liu, Y.; Liu, J.; Feng, G.; Yin, S.; Cen, W.; Liu, Y. Interface effects for the hydrogenation of CO_2 on Pt_4/γ-Al_2O_3. *Appl. Surf. Sci.* **2016**, *386*, 196−201.
(43) Deng, C.-M.; Huo, C.-F.; Bao, L.-L.; Feng, G.; Li, Y.-W.; Wang, J.; Jiao, H. CO Adsorption on Fe_4C (100), (110), and (111) Surfaces in Fischer−Tropsch Synthesis. *J. Phys. Chem. C* **2008**, *112*, 19018−19029.
(44) Kresse, G.; Hafner, J. Ab initiomolecular dynamics for liquid metals. *Phys. Rev. B: Condens. Matter Mater. Phys.* **1993**, *47*, 558.
(45) Kresse, G.; Hafner, J. Ab initiomolecular-dynamics simulation of the liquid-metal-amorphous-semiconductor transition in germanium. *Phys. Rev. B: Condens. Matter Mater. Phys.* **1994**, *49*, 14251.
(46) Kresse, G.; Furthmüller, J. Efficiency of ab-initio total energy calculations for metals and semiconductors using a plane-wave basis set. *Comput. Mater. Sci.* **1996**, *6*, 15−50.
(47) Kresse, G.; Furthmüller, J. Efficient iterative schemes forab initiototal-energy calculations using a plane-wave basis set. *Phys. Rev. B: Condens. Matter Mater. Phys.* **1996**, *54*, 11169.
(48) Dudarev, S. L.; Botton, G. A.; Savrasov, S. Y.; Humphreys, C. J.; Sutton, A. P. Electron-energy-loss spectra and the structural stability of nickel oxide: An LSDA+U study. *Phys. Rev. B: Condens. Matter Mater. Phys.* **1998**, *57*, 1505.
(49) Perdew, J. P.; Zunger, A. Self-interaction correction to density-functional approximations for many-electron systems. *Phys. Rev. B: Condens. Matter Mater. Phys.* **1981**, *23*, 5048.
(50) Perdew, J. P.; Burke, K.; Ernzerhof, M. Generalized Gradient Approximation Made Simple [Phys. Rev. Lett. 77, 3865 (1996)]. *Phys. Rev. Lett.* **1997**, *78*, 1396.
(51) Conejeros, S.; Alemany, P.; Llunell, M.; Moreira, I. d. P. R.; Sánchez, V.; Llanos, J. Electronic structure and magnetic properties of $CuFeS_2$. *Inorg. Chem.* **2015**, *54*, 4840−4849.
(52) Khalediali dusti, R.; Mishra, A. K.; Barnoush, A. Temperature-dependent properties of magnetic $CuFeS_2$ from first-principles calculations: Structure, mechanics, and thermodynamics. *AIP Adv.* **2019**, *9*, 065021.
(53) Pauling, L.; Brockway, L. O. The crystal structure of chalcopyrite $CuFeS_2$. *Z. für Kristallogr.—Cryst. Mater.* **1932**, *82*, 188−194.
(54) Hall, S. R.; Stewart, J. M. The crystal structure refinement of chalcopyrite, $CuFeS_2$. *Acta Crystallogr., Sect. B: Struct. Crystallogr. Cryst. Chem.* **1973**, *29*, 579−585.
(55) Kratz, T.; Fuess, H. Simultane Strukturbestimmung von Kupferkies und Bornit an einem Kristall. *Z. Krist.* **1989**, *186*, 167−169.
(56) Momma, K.; Izumi, F. VESTA 3 for three-dimensional visualization of crystal, volumetric and morphology data. *J. Appl. Crystallogr.* **2011**, *44*, 1272−1276.
(57) Kitchin, J. Free Software Foundation: Boston, 2008.
(58) Grimme, S. Semiempirical GGA-type density functional constructed with a long-range dispersion correction. *J. Comput. Chem.* **2006**, *27*, 1787−1799.
(59) Henkelman, G.; Arnaldsson, A.; Jónsson, H. A fast and robust algorithm for Bader decomposition of charge density. *Comput. Mater. Sci.* **2006**, *36*, 354−360.
(60) Bader, R. F. W. *Atoms in Molecules: A Quantum Theory*; Oxford University Press: London, 1994.
(61) Tasker, P. W. The stability of ionic crystal surfaces. *J. Phys. C: Solid State Phys.* **1979**, *12*, 4977.
(62) de Oliveira, C.; de Lima, G. F.; de Abreu, H. A.; Duarte, H. A. Reconstruction of the Chalcopyrite Surfaces-A DFT Study. *J. Phys. Chem. C* **2012**, *116*, 6357−6366.

DOI: 10.1021/acsomega.9b01988
ACS Omega XXXX, XXX, XXX−XXX